PHYSICAL REVIEW B **69**, 121413(R) (2004)

Spectroscopic characterization of Stone-Wales defects in nanotubes

Yoshiyuki Miyamoto,[1] Angel Rubio,[2] Savas Berber,[3] Mina Yoon,[3] and David Tománek[3]
[1]*Fundamental and Environmental Research Laboratories, NEC Corporation, 34 Miyukigaoka Tsukuba 305-8501, Japan*
[2]*Dpto. Física de Materiales, Facultad de Químicas, Universidad del País Vasco, Centro Mixto CSIC-UPV/EHU and Donostia International Physics Center (DIPC), 20018 San Sebastián, Spain*
[3]*Department of Physics and Astronomy, Michigan State University, East Lansing, Michigan 48824-2320, USA*
(Received 26 January 2004; published 25 March 2004)

We combined resonant photoabsorption and vibration spectroscopy with scanning tunneling microscopy (STM) to unambiguously identify the presence of Stone-Wales (SW) defects in carbon and boron nitride nanotubes. Based on extensive time-dependent *ab initio* density functional calculations, we propose to resonantly photoexcite SW defects in the infrared and ultraviolet regime as a means of their identification. Onset of nonradiative decay to a local defect vibration with a frequency of 1962 cm^{-1} serves as a fingerprint of such defects in carbon nanotubes. The bias dependence of the STM images shows distinct features associated with the presence of SW defects.

DOI: 10.1103/PhysRevB.69.121413 PACS number(s): 78.67.−n, 73.22.−f, 71.15.Qe

Since the discovery of fullerenes[1] and nanotubes,[2] topological defects—in particular adjacent pentagon/heptagon pairs, called Stone-Wales (SW) defects[3]—have been proposed to play a major role in the growth and subsequent annealing down to the structurally ordered ground state of carbon nanostructures. The SW defect also plays a key role, enabling large-scale structural rearrangements in graphitic networks.[4] It consists of a local $\pi/2$ rotation of a C-C bond, creating two pentagons and heptagons. This SW transformation is thought to play an important role during the growth of carbon nanostructures. Once formed, the pentagon/heptagons could move along the structure, creating either dislocation centers in regions of positive (pentagons) or negative (heptagons) Gaussian curvature, which ultimately lead to the closing of the nanostructure. Moreover, SW defects appear at the core of many relevant structural transformations governing, for example, the coalescence of fullerenes[5] and nanotubes,[4] the formation of pure intramolecular junctions for nanoelectronic devices,[6] and the onset of either plastic or brittle response of tubes subject to mechanical strain.[7] Furthermore, recent calculations show the possibility of SW defects also in boron nitride (BN) nanotubes,[8] in which B-B and N-N bonds would be formed. In this case, the SW defect causes the appearance of new electronic levels in the intrinsic band gap of the tube, which may enhance the observed field emission from BN tubes.[9]

In spite of the relevance and large amount of theoretical work on SW defects, their experimental identification has up to now been elusive, and only indirect evidence has been provided.[3,10] The high activation energy barrier of several electron volts for the bond rotation in nanotubes[4] would make the density of SW defects small in thermodynamic equilibrium. Still, these defects should occur as metastable structures at room temperature, and can be frozen in the nanotube body during the nonequilibrium growth process. Note that other energetically comparable, but much more visible defects, including isolated pentagons and heptagons (i.e., knees, bent tubes, *T* junctions), are often seen in transmission electron microscopy (TEM) images,[11] since these defects induce bending and reshaping of the entire nanotube structure at a relative small cost of elastic strain energy. In contrast to this, the mild structural deformation introduced by the SW defect prevents a proper identification by TEM, transport measurements, and/or electron spin resonance. Thus we have to rely on atomically resolved scanning tunneling spectroscopy (STM) to visualize and identify these rare defects.[12] It would be highly desirable to have an additional global characterization tool, which would identify the presence of SW defects along with the local identification by STM.

In this communication, we propose an unambiguous experimental identification of SW defects on bulk nanotube samples based on first-principles excited state electron-ion dynamic simulations. We show that photoexcitations in tubes with SW defects decay through a local vibration at the defect site. This vibration is distinguishable from the phonon modes of the defect-free tube, and can be used to characterize the presence of SW defects in the nanotube sample. Those results are complemented with simulations of STM images of SW defects in order to locally identify them.

Large-scale density functional theory (DFT) calculations were performed using norm-conserving pseudopotentials[13] to describe the electron-core interaction. Exchange-correlation effects are treated at the usual level of local-density approximation[14] (LDA). A plane wave cutoff of 40 Ry and 50 Ry was used to represent the valence wavefunctions for carbon and BN nanotubes, respectively. The structure of the tube with a single SW defect was simulated in a supercell geometry. This supercell is large enough to avoid spurious defect-defect and tube-tube interactions.[15] The defective-tube geometry, before photon excitation, is relaxed following the calculated atomic forces.[16] For the electron/ion dynamics after photoexcitation, we use the time-dependent density functional theory coupled to a molecular-dynamics technique (TDDFT-MD), following the Hellmann-Feynman forces on the excited system.[17] The photoexcitation process is simulated by selectively inducing a particle-hole excitation. For this configuration, keeping the ions fixed, we computed self-consistently the electronic excited states, from which the simulation of ion dynamics starts.

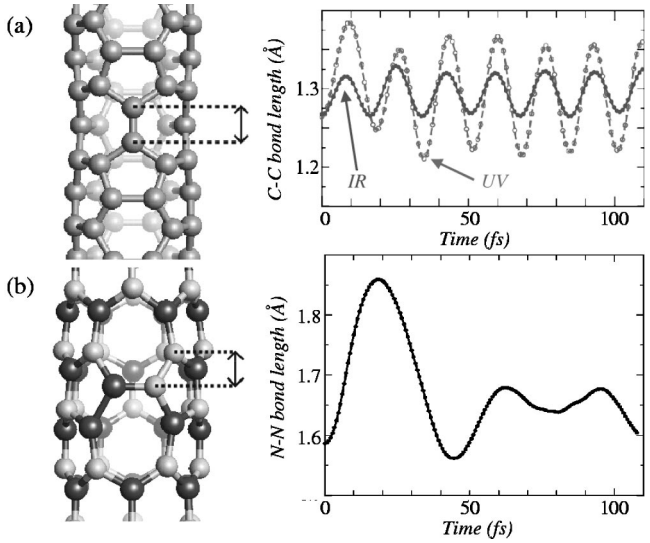

FIG. 1. (a) Left, fully relaxed structure of the SW defect for a C(3,3) tube. Right, time evolution of the central SW C-C bond length (along the tube axis) upon photoexcitation with infrared, 0.6 eV and ultraviolet, 6 eV light. (b) Left, fully relaxed structure of the a BN(6,0) tube with a SW defect. Right, time evolution of the N-N bond length of the SW defect upon photoexcitation from N-N σ to N-N σ^* (corresponding to a 12 eV excitation). Black and gray balls denote B and N atoms, respectively.

Local probes, such as STM (see the discussion below), allow to identify individual SW defects, but their use is not practical for large-scale investigations. Instead, resonant-vibrational spectroscopy (as, for example, resonant Raman scattering[18]) has been turned into a very precise, highly diameter selective identification tool of carbon nanotube samples. Here we go a step further, and address the detection of specific localized vibration modes of the SW defect. To achieve the high sensitivity needed for detecting this local vibration, we look for an enhancement of the coupling of photoexcited defect-related electronic states with local vibrations. We demonstrate that this photoenhancement mechanism is indeed efficient by first-principles (infrared and ultraviolet) photoinduced excited state dynamics calculations on a (3,3) carbon nanotube with a single SW defect (the diameter is only $\sim$4 Å, as those recently discovered either in a center of multiwall nanotube or in a zeolite matrix[20]). The choice of such a small diameter is to address the curvature effect in an extreme case and also to reduce the computational burden of the first principles TDDFT-MD simulation. Moreover, the results would remain valid for nanotubes with larger diameter.

The left panel of Fig. 1(a) shows the relaxed geometry of the (3,3) tube with one SW defect per four unit cells. The SW defect is set such that the C-C bond between heptagons is parallel to the tube axis. The relaxed C-C bond length is 1.27 Å, similar to the corresponding bond length of a SW defect in a planar graphene sheet.[21] However, this bond length increases to 1.40 Å when the C-C bond at the defect changes its orientation (geometry not shown here). This orientation dependence of the central C-C bond length is due to the high curvature of the narrow nanotube and gets much smaller in thicker nanotubes, where the C-C network of the SW defects converges to the corresponding structure on a graphene sheet.[22] We confirmed this is the case for the relaxed structure of a SW defect in a (10,10) carbon nanotube.

The time evolution of the SW central C-C bond length upon photoexcitation with either infrared (0.6 eV) or ultraviolet (6.0 eV) light is shown in the right panel of Fig. 1(a). The excitation energies were determined from two independent total-energy calculations, one for the electronic ground state and the other for an excited state configuration. This approach, $\Delta-$SCF, has been shown to work very well for describing excitations in low-dimensional structures.[19] In particular, the infrared excitation corresponds to promoting an electron from the π-state of the C-C bond to the corresponding excited π^* state. On the other hand, the ultraviolet excitation accounts for a transition from a C-C σ-π hybridized state to the previous C-C π^* unoccupied state.[23] By inspecting the results shown in the right panel of Fig. 1(a), we observe that the photoexcitation energy is very efficiently transferred into a localized vibration mode of the central C-C bond of the SW defect. Indeed, only after a few tens of fs is the amplitude of the vibration stabilized and the decay process completed. Despite the difference in excitation energies, both infrared and ultraviolet excitations induce local vibrations with exactly the same frequency[24] of 1962 cm^{-1}. This frequency coincides with the vibrational frequency in the corresponding electronic ground state and hence serves as a fingerprint of the presence of SW defect. Furthermore, the fact that this frequency is much higher than that of any tangential optical mode of nanotubes of $\approx$1580 cm^{-1} indicates that the lifetime of this localized mode with respect to phonon-phonon scattering should be rather long and thus easy to observe following the photoexcitation.[25] As the electron-hole pairs, which are responsible for the resonant process, are very localized on the π and π^* orbitals of the SW bond defect, the metallic or semiconducting character of the host nanotube does not alter the otherwise low decay of this excitation into valence or conduction nanotube states. The optical signal can be increased by scanning along the nanotube with a scanning-near-field-optical microscope (SNOM).

Due to the success of the photoexcitation technique in carbon nanotubes, we looked at the possibility of detecting SW defects in BN tubes through a similar process. In the left panel of Fig. 1(b), we show the fully relaxed geometry of a BN(6,0) nanotube, where B-B and N-N bonds are formed. We have selected a zig-zag geometry for the BN nanotube, because experimentally this seems to be the predominant chirality.[26] In the right panel of Fig. 1(b) we show the time evolution of the central N-N bond length, triggered by the 12 eV photoexcitation from the N-N σ to the N-N σ^* state. In contrast to carbon nanotubes, the excited state dynamics shows a rapid decay of the N-N vibration amplitude. This is the general trend found in all simulations performed for BN tubes. More detailed analysis of the electron dynamics indicates a rapid delocalization of the N-N σ and σ^* states, which weakens the force constant of the central N-N bond throughout the simulation. This quick delocalization is most likely related to a stronger electron-phonon coupling and in-

elastic phonon-phonon scattering in BN nanotubes than in carbon nanotubes, due to the polar nature of the BN bond. This stronger-electron phonon coupling might be relevant in the electron transport properties of doped BN tubes.[27] Therefore, photoexcited vibrational spectroscopy in BN tubes should be less efficient as a fingerprint of SW defects, leaving more local probes, including the STM, as the only alternatives.

The global characterization tool for SW defects in carbon nanotube samples described above should be complemented with a local probe, such that information about the spatial localization of the SW defect can be extracted. This can be achieved by recording the STM image of the defective tube. In the simplest approximation,[28] the STM current for an external applied bias voltage V is directly proportional to the spatial local density of states at the tip center, integrated between the Fermi level of the tip and sample, as $\mathcal{I}(\mathbf{r},V) \propto \int_{E_F^s}^{E_F^s+eV} dE \Sigma_{nk} |\psi_{nk}(\mathbf{r})|^2 \delta(E_{nk}-E)$, where ψ_{nk} are the Kohn-Sham eigenfunctions of the tube, and nk denotes the band index for each k point of the 1D Brillouin zone of the tube. Thus, we simulate STM images as isosurfaces of constant $\mathcal{I}$.[29]

The results of our constant current STM simulations for applied bias potential of ± 1.5 eV are presented for the armchair (10,10) carbon nanotube in Fig: 2(a) and the zigzag boron nitride (6,0) tube in Fig. 2(b). Note that the small diameter carbon tube, shown in Fig. 1(a), is marginally stable. Although the results of the photoexcitation process are valid for larger tubes, inspection of STM images of the more common (10,10) nanotube is more relevant. We have performed simulations for nanotubes with different chiralities, diameters, and orientations of the C-C (N-N) bond of the SW defect (parallel, perpendicular, and tilted to the tube axis). All simulations exhibit similar features as those shown in Figs. 2(a) and (b). First of all, the SW defect creates a very localized modification of the STM image as compared to a perfect tube (the decay length of the perturbation is very short, few unit cells). Second, the left (right) panels of Fig. 2 show that the symmetry of the image corresponding to occupied (unoccupied) states is completely different. For a carbon nanotube we obtain clear protrusions at the pentagonal sites, which exhibit, as a function of bias polarity, different nodal structures with respect to the central C-C bond. The simulated STM images are consistent with a recent measurement[10] and with previous calculations without atomic relaxations.[12] For the (6,0) BN nanotube, the STM image at ± 1.5 eV clearly probes the defect states located in the gap of the BN tube, which correspond to the occupied π N-N bond and the unoccupied π^* B-B bond. Increasing the negative (positive) bias produces an image with protrusions located at the N (B) atoms (triangular symmetry, in contrast to the hexagonal lattice of carbon nanotubes), in agreement with recent experiments.[30] All the calculations clearly indicate that the SW defect can be, indeed, experimentally accessible by STM measurements and 3D mapping (as done in Ref. 31 for carbon nanotubes). Experimentally this is a very hard task, as the defect should be properly oriented with respect to the STM tip. This limitation is not present in the resonant-vibrational spectroscopy discussed above.

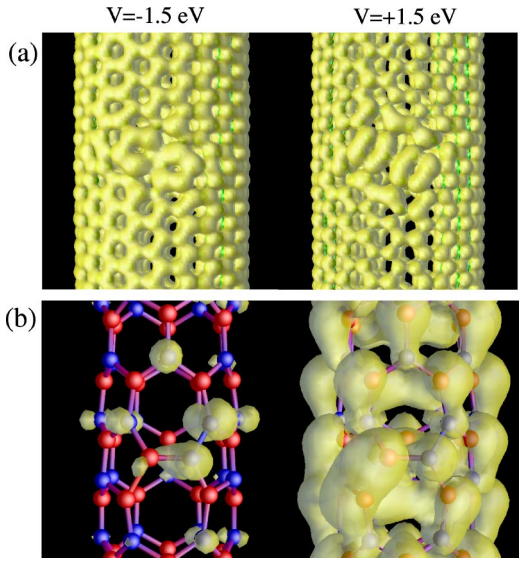

FIG. 2. (Color online) Simulated constant current STM images for (a) C(10,10) and (b) BN(6,0) nanotubes with a single SW defect, for applied external tip-sample bias of ± 1.5 eV. The orientation of the centered bond joining the two pentagons of the SW defect is set to $\pi/4$ degrees to the tube axis in the case of the carbon nanotube and perpendicular to the tube axis in the case of the BN nanotube. SW-defect states in the BN band gap are clearly seen (with N-N π and B-B π^* character for negative and positive bias, respectively). C, B and N atoms are depicted in green, red, and blue, respectively.

In conclusion, we have proposed an efficient way to identify SW defects in carbon nanotubes that complements local probes including STM, namely the induction of a defect-localized vibration by photoexcitation. This technique can also be used to monitor the formation of SW defects during nanotube growth. We have shown that this approach is less effective in BN tubes due to the polar nature of the BN bond, which reduces the lifetime of the localized vibrations. In both C and BN tubes, local STM images provide unambiguous evidence of the corresponding topological defects.

Part of the calculations were performed in the SX4 Supercomputer System at the NEC Tsukuba Laboratory, the SX5 Supercomputer Systems at the National Institute of Materials Science and the NEC Fuchu Plant. Y.M. was supported by NAREGI Nanoscience Project, Ministry of Education, Culture, Sports, Science and Technology, Japan. A.R. acknowledges support from the EC grants (HPRN-CT-2000-00128 and HPRN-CT-2000-00167) and Spain MCyT. M.Y. and D.T. acknowledge partial support by NSF-NIRT grant DMR-0103587.

[1] H.W. Kroto, J.R. Heath, S.C. O'Brien, R.F. Curl, and R.E. Smalley, Nature (London) **318**, 162 (1985).
[2] S. Iijima, Nature (London) **354**, 56 (1991).
[3] A.J. Stone and D.J. Wales, Chem. Phys. Lett. **128**, 501 (1986).
[4] M. Yoon, S. Han, G. Kim, S. Lee, S. Berber, E. Osawa, J. Ihm, M. Terrones, F. Banhart, J-C. Charlier, N. Grobert, H. Terrones, P.M. Ajayan, and D. Tománek, Phys. Rev. Lett. **92**, 075504 (2004).
[5] Y.H. Kim, I.H. Lee, K.J. Chang, and S. Lee, Phys. Rev. Lett. **90**, 065501 (2003); Y. Zhao, B.I. Yakobson, and R.E. Smalley, *ibid.* **88**, 185501 (2002); H. Ueno, S. Osawa, E. Osawa, and K. Takeuchi, Fullerene Sci. Technol. **6**, 319 (1998); S. Han, M. Yoon, S. Berber, N. Park, E. Osawa, J. Ihm, and D. Tománek (unpublished).
[6] M. Ouyang, J.L. Huang, C.L. Cheung, and C.M. Lieber, Science **291**, 97 (2001); V.H. Crespi, M.L. Cohen, and A. Rubio, Phys. Rev. Lett. **79**, 2093 (1999).
[7] M.B. Nardelli, B.I. Yakobson, and J. Bernholc, Phys. Rev. Lett. **81**, 4656 (1998).
[8] H.F. Bettinger, T. Dumitricä, G.E. Scuseria, and B.I. Yakobson, Phys. Rev. B **65**, 041406(R) (2002).
[9] P. Dorozhkin, D. Golbert, Y. Bando, and Z.C. Dong, Appl. Phys. Lett. **81**, 1083 (2002); J. Cummings and A. Zettl, in *Electronic Properties of Molecular Nanostructures* (AIP, Melville, New York, 2001), p. 577; Y. Miyamoto and A. Rubio (unpublished).
[10] Ali Yazdani (private communication).
[11] S. Iijima, T. Ichihashi, and Y. Ando, Nature (London) **356**, 776 (1992).
[12] A. Rubio, Appl. Phys. A: Mater. Sci. Process. **68**, 275 (1999); D. Orlikowski, M.B. Nardelli, J. Bernholc, and C. Roland, Phys. Rev. B **61**, 14 194 (2000).
[13] N. Troullier and J.L. Martins, Phys. Rev. B **43**, 1993 (1991).
[14] D.M. Ceperley and B.J. Alder, Phys. Rev. Lett. **45**, 566 (1980).
[15] The supercell used to describe the SW defect in the tube consists of a periodic array of tubes having an interwall distance of 4 Å. The unit cell along the tube axis is set to four perfect armchair unit cells. We have checked the convergence of our results by increasing the cell size.
[16] Although the activation barrier for bond rotation in carbon nanotubes lies between 5 and 8 eV, the SW defect formation energy in a C(3,3) tube is 1.03 eV. This low value results from the extra flexibility of the narrow tube, which reduces the amount of long-range strain energy present in planar graphite (Ref. 22). The strain energy per atom is 0.43 eV in a perfect C(3,3), and 0.29 eV in BN(3,3).
[17] O. Sugino and Y. Miyamoto, Phys. Rev. B **59**, 2579 (1999); **66**, 089901(E) (2002); M.A.L. Marques, A. Castro, G.F. Bertsch, and A. Rubio, Comput. Phys. Commun. **151**, 60 (2003).
[18] See M.S. Dresselhaus, G. Dresselhaus, A. Jorio, A.G. Souza Filho, and R. Saito, Carbon **40**, 2043 (2002), for a review on resonant Raman spectroscopy of carbon tubes including vibrational modes related to defects.
[19] R.O. Jones and O. Gunnarsson, Rev. Mod. Phys. **61**, 689 (1989); G. Onida, L. Reinig, and A. Rubio, *ibid.* **74**, 601 (2002); M.A.L. Marques and E.K.U. Gross, in *A Primer in Density Functional Theory*, Lecture Notes in Physics 620 (Springer Verlag, Berlin, 2003).
[20] L. Qin, X. Zhao, K. Hirahara, Y. Miyamoto, Y. Ando, and S. Iijima, Nature (London) **408**, 50 (2000); N. Wang, Z.K. Tang, G.D. Li, and J.S. Chen, *ibid.* **408**, 50 (2000).
[21] S. Letardi, M. Celino, F. Cleri, and V. Rosato, Surf. Sci. **496**, 33 (2002).
[22] E. Kaxiras and K.C. Pandey, Phys. Rev. Lett. **61**, 2693 (1988).
[23] The pronounced σ-π hybridization is induced by the high local curvature of the (3,3) nanotube [X. Blase, L.X. Benedict, E.L. Shirley, and S.G. Louie, Phys. Rev. Lett. **72**, 1878 (1994)].
[24] When the SW defect is oriented at an angle with respect to the (3,3) tube axis, the calculated vibrational frequency of 1962 cm^{-1} upon infrared photoexcitation is shifted to 1450 cm^{-1} due to curvature effects (strong π-σ hybridization for this very small tube). However, for diameters above 1 nm, as commonly observed in experiments with single-wall tubes (Ref. 2), the computed local vibration frequency of 1962 cm^{-1} is rather insensitive to tube chirality and relative orientation of the SW defect (now curvature plays a very small effect on the frequency as we are dealing with σ-like bonding).
[25] The amplitude of the induced vibration is higher for the ultraviolet than for the infrared excitation. As our simulations treat the ions classically, this information only provides evidence about the average amount of energy transfered to the local vibration and not about the discrete vibrational level structure, as one would get from a full quantum mechanical treatment, which is beyond the scope of the present work.
[26] R.S. Lee, J. Gavillet, M. Lamy de la Chapelle, A. Loiseau, J.-L. Cochon, D. Pigache, J. Thibault, and F. Willaime, Phys. Rev. B **64**, 121405(R) (2001). HRTEM analysis show a zigzag configuration for most SWNTs in agreement with previous results on MWNT's [D. Goldberg, Y. Bando, W. Han, K. Kurashima, and T. Sato, Chem. Phys. Lett. **308**, 337 (1999)].
[27] M. Radosavljević, J. Apenzeller, V. Derycke, R. Martel, Ph. Avouris, A. Loiseau, J.L. Cochon, and D. Pigache, Appl. Phys. Lett. **82**, 4131 (2003).
[28] J. Tersoff and D.R. Hamann, Phys. Rev. Lett. **50**, 1998 (1983).
[29] Although tip-convolution effects are neglected, the general shape of the STM-image remains unchanged [V. Meunier and P. Lambin, Phys. Rev. Lett. **81**, 5588 (1998)].
[30] The large band gap of BN tubes makes STM imaging very difficult, since the large bias voltages needed could cause local Coulomb explosion. Still, the predicted triangular lattice STM image for BN tubes has recently been observed in low temperature STM by M. Ishigami, S. Aloni, and A. Zettl, in Proceedings of the XVIIth Winterschool on Electronic Properties of Novel Materials (AIP, New York, 2003).
[31] S.G. Lemay, J.W. Janssen, M. van den Hout, M. Mooij, M.J. Bronikowski, P.A. Willis, R.E. Smalley, L.P. Kouwenhoven, and C. Dekker, Nature (London) **412**, 617 (2001).